ADVANCED FUNCTIONAL MATERIALS
www.afm-journal.de

Ultra-Thin Self-Assembled Protein-Polymer Membranes: A New Pore Forming Strategy

*Patrick van Rijn, Murat Tutus, Christine Kathrein, Nathalie C. Mougin, Hyunji Park, Christopher Hein, Marco P. Schürings, and Alexander Böker**

Self-assembled membranes offer a promising alternative for conventional membrane fabrication, especially in the field of ultrafiltration. Here, a new pore-making strategy is introduced involving stimuli responsive protein-polymer conjugates self-assembled across a large surface area using drying-mediated interfacial self-assembly. The membrane is flexible and assembled on porous supports. The protein used is the cage protein ferritin and resides within the polymer matrix. Upon denaturation of ferritin, a pore is formed which intrinsically is determined by the size of the protein and how it resides in the matrix. Due to the self-assembly at interfaces, the membrane constitutes of only one layer resulting in a membrane thickness of 7 nm on average in the dry state. The membrane is stable up to at least 50 mbar transmembrane pressure, operating at a flux of about 21 000–25 000 L m^{-2} h^{-1} bar^{-1} and displayed a preferred size selectivity of particles below 20 nm. This approach diversifies membrane technology generating a platform for "smart" self-assembled membranes.

1. Introduction

Self-assembled membranes are a promising alternative for those produced via high resolution methods such as X-ray, electron beam and interference lithography.[1–3] Not only are these methods limited with respect to generating low nanometer pore sizes, there is also a high cost associated with production. Recently, a drive to develop new approaches for membrane preparations provided ultra-thin membranes completely based on self-assembly.[4,5] These membranes rely on the use of either nanoparticles,[6,7] proteins,[8,9] small molecular species[10,11] or block-copolymers.[12,13] Although, these membrane structures display high flux, good selectivity or thicknesses in the low nanometer regime: permeation area is limited. Moreover, self-assembly of hybrid protein-polymer structures allows for advanced control over membrane properties such as pore-size and responsiveness towards external stimuli, creating smart ultra-thin hybrid membranes. In the past, the insertion of trans-membrane protein channels into the walls of polymersomes were used to produce interesting switchable nano-containers.[14,15] The number of pores in the polymersomes was adjusted by changing the polymer-channel ratio and up to 25 protein channels per polymer vesicle could be achieved.[16] In terms of membrane based separation processes, higher chemical selectivity through controlled pore-size and shape or alteration of the permeability by an external stimulus are desirable for drug delivery,[17,18] (bio-)reactive membrane systems[19] and enantio-selective separations.[20,21] In addition, the reduction of the membrane thickness is essential to achieve higher throughput at lower applied pressures and to increase the membrane performance. However, membrane thicknesses of a few nanometers are difficult to achieve with proper mechanical robustness and controlled pore-sizes. It has to be noted that mechanically robust membranes in the lower nanometer regime ranging from 10 nm to 150 nm with better defined pore-diameters have been developed based on lithography.[22,23] This is a time and energy inefficient approach and achieving the same characteristic using a self-assembly approach would be desirable but is still highly challenging. Here we present an approach which enables large area ultra-thin, yet robust, membranes to be formed. The membrane is composed of a ferritin-polymer core-shell microgel-like structure which self-assembles at polar-apolar interfaces.[24] Core-shell microgel structures are excellent soft particles for the formation of macroscopic structures in a controlled fashion, incorporating stimuli-responsive

Dr. P. van Rijn, Dr. M. Tutus, C. Kathrein,
Dr. N. C. Mougin, H. Park, C. Hein,
M. P. Schürings, Prof. A. Böker
DWI-Leibniz-Institute for Interactive Materials
RWTH Aachen University
Forckenbeckstrasse 50, D-52056 Aachen, Germany
E-mail: boker@dwi.rwth-aachen.de
Dr. P. van Rijn, C. Kathrein, Dr. N. C. Mougin, H. Park,
M. P. Schürings, Prof. A. Böker
Lehrstuhl für Makromolekulare Materialien und Oberflächen
RWTH Aachen University
Forckenbeckstrasse 50, D-52056 Aachen, Germany
Dr. P. van Rijn
University of Groningen
University Medical Center Groningen
Department of Biomedical Engineering-FB40
W. J. Kolff Institute for Biomedical Engineering and Materials Science
A. Deusinglaan 1, 9713, AV, Groningen, The Netherlands
Dr. M. Tutus, C. Hein
Aachener Verfahrenstechnik
RWTH Aachen University
Turmstrasse 46, D-52056, Aachen, Germany

DOI: 10.1002/adfm.201401825

properties.[25,26] Ferritin (Horse spleen ferritin, HSF) is an iron storage protein in mammals and consists of a dodecameric protein cage of 12 nm in diameter with a 6 nm central cavity containing a phosphate ferrihydrite core.[27] The protein cage is stable over a large pH range and temperatures up to 60 °C in water and can tolerate organic co-solvents. Located externally are 72 chemically addressable primary amino-groups which were heretofore used for bioconjugation of dyes as well as polymers.[28,29] Due to the multi-component nature of ferritin, denaturation will induce a more open channel compared to when a single component protein structure is used. The formed membrane was tested with respect to stability and permeability and showed remarkable elasticity and mechanical robustness with a size selectivity preference for nanoparticles below 20 nm.

2. Results and Discussion

The conjugate, when self-assembled at polar-apolar interfaces, provides a monolayer of proteins which are surrounded by a polymer matrix consisting of a random copolymer of the thermo-responsive *N*-isopropylacrylamide (NIPAAm) and the UV-cross-linkable *2*-(dimethyl maleinimido)-*N*-ethyl-acrylamide (DMIAAm) (**Scheme 1**). Because both the protein and the polymer are deformable structures, upon assembly and subsequent cross-linking, a flexible and hence resilient membrane is formed. The protein is used as a sacrificial template and structural integrity is lost upon applying denaturing conditions such as high concentrations of urea or guanidinium chloride at elevated temperature. The loss of protein integrity induces pore-formation and the pore diameter depends on the size of the protein. Using an air-water interface for assembly followed by UV-cross-linking and slow evaporation of the aqueous phase, a 5 nm thin membrane will be formed. After protein denaturation, individual pores are created without compromising the overall membrane integrity. This method allows for an effective filtration area of ≈5 cm^2 to be formed and filtration parameters with regard to trans-membrane mass transport and size-selectivity can be conveniently manipulated using the temperature responsiveness of the polyNIPAAm component. These membranes have been tested in an in-house developed flow station allowing the system to be controlled via hydrostatic pressure (trans-membrane pressure (TMP) 3–50 mbar) with the trans-membrane pressure measured in situ. Size selectivity was determined using various sizes of gold nanoparticles and the collected filtrate was analyzed using spectrophotometry and transmission electron microscopy (TEM).

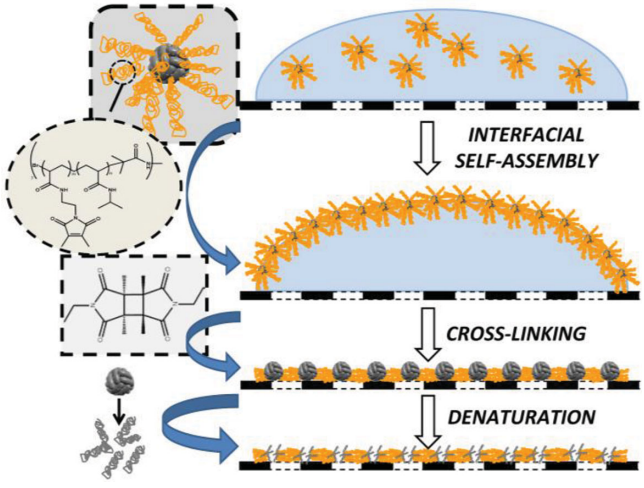

Scheme 1. Schematic overview of the formation of the protein-polymer hybrid membrane.

The drying-mediated membrane formation is based on the interfacial self-assembly properties of the protein-polymer particles, that is, the Pickering effect. This has been demonstrated by pendant-drop tensiometry analysis for air-water interfaces and the effect has been recently used for creating proto-cell structures.[30,31] By placing a drop of highly diluted protein-polymer particle solution (≈10 μg mL^{-1}) onto a solid support either porous or non-porous a membrane is formed via self-assembly at the water-air interface. At this concentration the particles assemble at the interface almost instantaneously to minimize air-water interaction energies (Scheme 1) and it was experimentally found that this concentration provides a monolayer arrangement and a complete surface coverage.[3,29,33] The particles at the interface are then irradiated with UV-light in order to induce inter-particle cross-linking. During irradiation, the sample is cooled on ice in order to keep the temperature below the lower critical solution temperature (LCST, 32–35 °C) of the polyNIPAAm. By cooling and irradiation over a period of 3 hours, the water slowly evaporates leaving behind the dry cross-linked protein-polymer membrane. In the case of a porous support, it was placed on a hydrophobic surface in order to minimize possible capillary forces which potentially draw the solution into the pores.

2.1. Membrane Formation

Self-assembly of the protein-polymer particles at the interface and the subsequent stabilization via inter-particle cross-linking by UV-irradiation was visualized using a benzotrifluoride-water interface. Benzotrifluoride was used because of the higher density compared to water which facilitates addition of the particles and washing of the top-phase, thereby removing any non-assembled particles. The particles were added to the aqueous top-phase and allowed to assemble overnight. After the assembly, 75% of the aqueous phase was removed and replaced with pure water. This procedure was repeated 3 times to remove residual particles not bound to the interface. UV-irradiation induced inter-particle cross-linking and stabilizes the formed protein-polymer particle layer. Subsequently, a benzotrifluoride droplet (colored with Nile Red) was placed onto the self-assembled cross-linked or non-cross-linked protein-polymer membrane to visualize the enhanced stability upon cross-linking. The droplet was put onto the non-cross-linked membrane and fell through the interface (**Figure 1**, non-cross-linked; inset) while the cross-linked membrane kept the droplet on the interface without recombining with the benzotrifluoride sub-phase (Figure 1, cross-linked). The membrane was able to endure mechanical stress without rupturing as the droplet can even be pushed onto the membrane resulting in deformation of the droplet instead of passing through the particle-stabilized

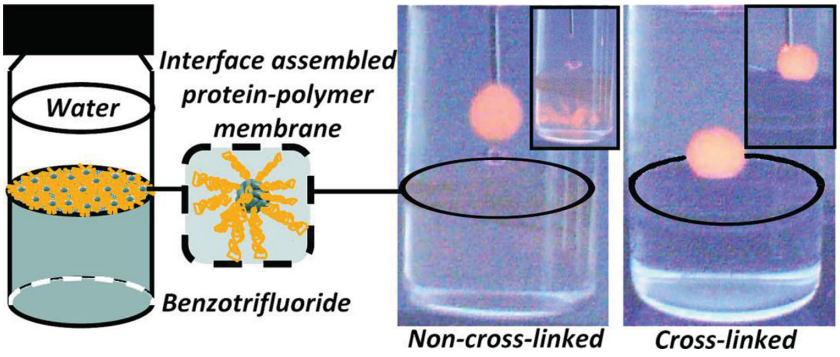

Figure 1. The strength and flexibility of the self-assembled membrane is shown by introducing an oil droplet (benzotrifluoride, containing Nile Red as a fluorescent dye) onto it which is formed in between oil (benzotrifluoride; bottom) and water (top). The non-cross-linked and cross-linked case displays a significant difference in stability.

interface (Figure 1, cross-linked; inset). To visualize the membrane, a fluorescent comonomer (fluorescein-acrylate) was introduced during the protein-polymer particle preparation[32] and the interface was transferred onto a glass substrate. Fluorescence microscopy shows the presence of the membrane (S1, Supporting Information).

As shown in Figure 1, the membrane was easily formed at a polar-apolar interface which can be oil-water as well as air-water. To prevent potential damage during membrane transfer after formation, the preferred approach for formation is directly on the supporting material as described in Scheme 1. The process was performed on bare silicon oxide to characterize the formed layer produced via the drying-mediated self-assembly method which was also used to cover the porous support needed for the trans-membrane measurements.

The protein-polymer layer formed via drying-mediated self-assembly was analyzed using ellipsometry and scanning force microscopy (SFM). According to ellipsometry measurements, the protein-polymer membrane was on average approximately 7.5 nm (±1.3 nm) thick in the dry state. The measured thickness was composed of protein and polymer and while the protein is 12 nm in diameter, the polymer layer should therefore be thinner. This was confirmed by SFM analysis. The protein-polymer membrane displayed a homogeneous coverage of the substrate with some agglomeration (**Figure 2**A). The proteins are shown as bright spots in the height profile analysis, indicating that indeed they rise above the surrounding polymer matrix. The membrane was partially removed by scratching with a cannula in order to determine the actual thickness of the cross-linked polymer matrix. The transition between membrane covered silicon substrate and non-covered substrate was investigated by SFM analysis, and the height profile indicated a polymer-layer thickness of about 5 nm (Figure 2B,C). This was in good agreement with the layer thickness found by ellipsometry. The presence of ferritin in the polymer matrix was also confirmed by transmission electron microscopy (TEM) analysis by applying the same method as for the silicon substrate but using a TEM-grid. The iron core

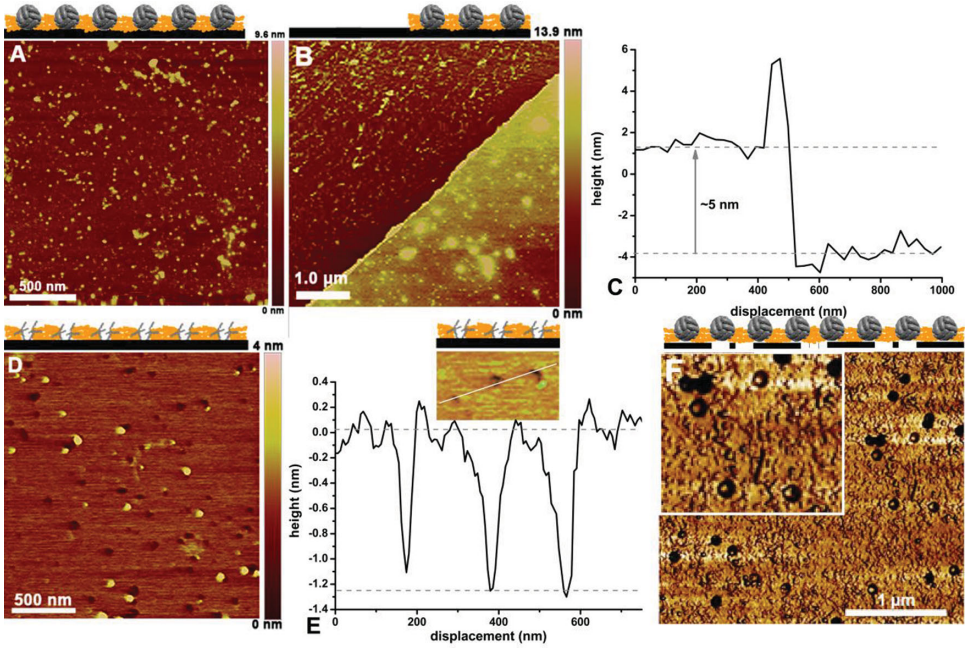

Figure 2. SFM analysis of the drying-mediated self-assembled protein-polymer membrane. A) Proteins surrounded by the cross-linked polymer matrix on a silicon wafer. B,C) The protein-polymer membrane is about 5 nm thick as illustrated by height analysis of a scratched substrate. D) The protein is selectively denatured by treatment with 8 M urea solution at elevated temperature, leaving behind an open pore-like structure. E) The depth was shown to be approximately 2 nm, determined by SFM height analysis (line in inset indicates position of profile). F) This membrane formation technique was also used in combination with a porous support (PC-membrane, pore-size 100 nm) to make it suitable for trans-membrane flow experiments. For membrane characterization, protein structures were found also to span across the membrane support pores (inset).

inside the ferritin cage is clearly visible by TEM (S2, Supporting Information).

To create hydrophilic pores, the ferritin was denatured in order to remove all secondary and tertiary protein structure. The removal of the secondary and tertiary structure is expected to create a pore but without removal of the actual cage fragments because these are covalently connected to the polymer matrix. Denaturation of ferritin is conventionally done using highly concentrated aqueous urea solutions in combination with SDS (sodium dodecylsulfonate) at elevated temperatures or using guanidinium chloride at high temperatures. In order to investigate the minimum requirements for denaturing the ferritin, the native ferritin and protein-polymer conjugate were both subjected to various denaturing conditions to monitor the secondary structure using gel electrophoresis and circular dichroism (S3, S4, Supporting Information). From gel electrophoresis analysis it was shown that both guanidinium chloride at pH 4.4 as well as urea (8 M) at 90 °C for 3 h were satisfactory conditions for denaturing the cage structure of the ferritin in a 1 mg mL^{-1} solution, indicated by the loss of signal of the native mass of ferritin (440 kD). Urea was not used in combination with SDS, as is often the case in protein denaturation, because this could eventually interfere with the membrane, for example, detachment from the support surface or accumulation inside the pores due to coordination of SDS to the protein fragments. In order to investigate the protein-polymer conjugate, gel electrophoresis was not appropriate due to aggregation upon denaturation and hence did not run in the gel. Therefore Circular Dichroism (CD) measurements were used to monitor changes in the ferritin structure. Both native ferritin and ferritin-polymer conjugate displayed the same loss in CD signal after treatment with urea at 90 °C. The CD-signal which corresponds to the α-helix structural motif is abundantly present in ferritin.[33] With increasing denaturation time, it was found that a 3 h treatment was sufficient for complete denaturation, displaying a complete loss of the α-helix signal and appearance of random coil conformation.

The same procedure for denaturation was applied to the self-assembled membrane as shown in Figure 2A. Denaturation was achieved by covering the substrate holding the membrane with the urea solution and placing it in an oven at 90 °C. Although, for denaturation in solution 3 h was considered optimal, for pore formation inside the thin film, 45 min was sufficient which was determined experimentally. The reason can be that the amount of ferritin is many at least 100 times lower than the solution measured with circular dichroism and therefore less denaturation time is needed. As shown in Figure 2D, pore-like structures appear while the protein structures as observed in Figure 2A are no longer present. From the height profile across the pores, the depth could be determined to be approximately 1–2 nm (Figure 2E). This seems less than the thickness of the polymer layer and can be explained by the fact that the SFM tip used (with a diameter of typically 20 nm) is not expected to tap through the whole pore. Also the pore diameter in the SFM images is not exactly the same size as the protein but larger than anticipated. This can be explained by the pore-formation mechanism: ferritin is composed of 24 subunits held together via non-covalent interactions. Upon denaturation, the subunits are detached from each other inducing local loss of integrity within the membrane where the ferritin resides. Due to tension building-up on the polymer-ferritin bonds during denaturation at elevated temperatures the subunits will be pulled away from one another and the pore is formed. Since the peptide strand still resides inside the pore due to the covalent bond, the actual pore is probably smaller than observed by SFM which will become apparent from the size cut-off experiments as shown later. When a shorter polymer chain attached to the ferritin is used, the pore density increases but with it also the chance of pore recombination, forming larger pores (Figure S5, Supporting Information). The formation of the pores under the denaturing conditions also indicates a high stability of the membrane since 90 °C is well above the operating temperature and the LCST. The polymer matrix remains stable which also became clear from procedures followed using a ferritin-polymer conjugate with shorter chains which were due to the high pore density not suitable for use as a membrane but clearly show control over pore density and polymer matrix stability (S5). In order to test the membrane, the same procedure was repeated but instead of a planar silicon oxide support, a polycarbonate (PC) membrane with pore diameter of 100 nm was used. SFM analysis of the porous support with the formed self-assembled membrane on top via the same method as for the formation on silicon oxide displayed ferritin molecules with some directly over the pore, indicating a successful formation of the protein-polymer membrane (Figure 2F).

2.2. Membrane Characterization and Selectivity

The protein-polymer membrane was tested in a specially designed flow-station which operates on hydrostatic pressure (S6, Supporting Information). The flow-cell was designed in such a way that trans-membrane pressures could be measured and that the analytes for separation could be injected close to the membrane to minimize amounts of analyte. The protein-polymer membrane was tested for water-flux across the membrane before and after protein denaturation at 20 °C and 40 °C. The polyNIPAAm matrix exhibits a LCST of about 32–35 °C, above this temperature the polymer matrix becomes dehydrated and therefore less permeable to water as well as analytes. In the hydrated state, the polymer-gel layer was permeable[34] and hence switching temperature would allow for easy membrane cleaning.

2.2.1. Membrane Flux Determination

In order to test the membrane formation as well as the membrane's stability, flux measurements (water transport) were conducted at varying trans-membrane pressures (TMP) for the non-denatured protein-polymer membrane. The measurement consisted of a cyclic measurement going from low TMP to higher TMP and back again (**Figure 3**). Both the porous support and the support covered with the protein-polymer membrane were analyzed. The measured membrane area was ≈5 cm^2 which is a large area relative to the thickness of the protein-polymer membrane and usually areas much smaller are used.[35,36] The protein-polymer membrane was formed directly on the porous support by using an "O"-ring as a barrier with a thin layer of grease to prevent any solution escaping during

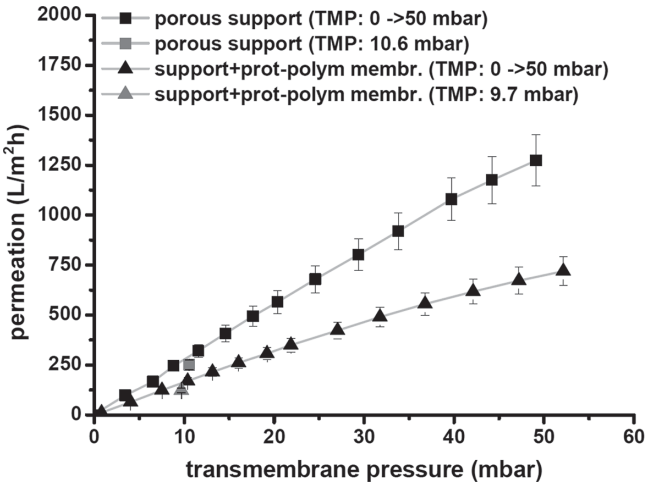

Figure 3. The protein-polymer membrane was assembled on top of a porous support as shown in Scheme 1. Both the porous support and the support with the non-denatured protein-polymer membrane were characterized with respect to water-flux depending on the trans-membrane pressures (TMP) which was increased from 0 to 50 mbar. Subsequently, the pressure was reduced to 10.6 and 9.7 mbar for the porous support and support+protein-polymer membrane to verify membrane integrity and performance.

membrane formation and cross-linking. The preparation was performed with the support placed on a flat Teflon sheet as a hydrophobic barrier to prevent water leaking away through the membrane during preparation. The water flux increased with increasing TMP (Figure 3) which was controlled hydrostatically. The TMP was changed from 0–50 mbar and subsequently lowered to prove stability. For the support, the flux increased steadily until ≈1400 $L^1m^{-2}h^{-1}$ at 50 mbar and upon lowering to 10.6 mbar, the flux provided a similar value as before indicating a stable membrane. The same experiment was repeated for the support with the self-assembled protein-polymer membrane. The flux again displayed a steady increase with increasing TMP to approximately 700 $L^1m^{-2}h^{-1}$ at 50 mbar. Upon reducing the pressure to 9.7 mbar, the flux displayed a similar value as found for the initial measurement. The recovery of the same value indicates that the membrane remains intact and is stable during the course of the measurement. The thin protein-polymer membrane reduces the flux but not to a great extent, that is, the water is able to flow without excessive inhibition but enough to be detected. This is expected of an ultra-thin membrane and is an attractive feature for membrane-based purification systems. The permeation development against the TMP is not completely linear and levels of to some extent. As observed in Figure 3, the support with the protein-polymer membrane deviated more from linearity than the support alone. This effect can be explained by compressibility, compression of the membrane induces a lowered permeation which is more pronounced for the support with the protein-polymer membrane indicating the presence of a soft polymeric hydrogel-like layer.

2.2.2. Membrane Selectivity Towards PEG

In order to test size selectivity, the support, as well as the protein-polymer membrane before and after denaturation was used in combination with a mixture of linear polyethyleneglycols (PEG) (solution composition: 1:1 volume ratios of 1 g^1L^{-1} containing PEG: 200, 1000, 4000, and 20 000 Da). The measurement was performed at constant TMP of 9 mbar over a period of 120 min for both 20 °C and 40 °C, temperatures below and above the LCST of polyNIPAAm respectively (**Figure 4**A/B). In all cases, a constant flux was measured for 120 min (conventionally this is performed for less than 1 min) meaning that the membranes remained stable and that there was no significant fouling or damage to the membrane using the aqueous PEG solution. At 20 °C, the highest flux was found for the support (≈3.0×10^4 $L^1m^{-2}h^{-1}bar^{-1}$) and decreased for the protein-polymer membrane (≈2.1×10^4 $L^1m^{-2}h^{-1}bar^{-1}$). The flux for the denatured and non-denatured membrane was the same within the error margin meaning that the created pores did not significantly increase the permeability of the system. This can be explained by the fact that at 20 °C the polymer matrix is highly swollen and permeable for the water and that therefore in all cases the transport mainly takes place through the polymer matrix. However, this changes when increasing the temperature above the LCST which expels the water from the polymer matrix and lead to its collapse, finally sealing the matrix. Although, complete sealing of the matrix and hence completely expelling water cannot be stated since the matrix is

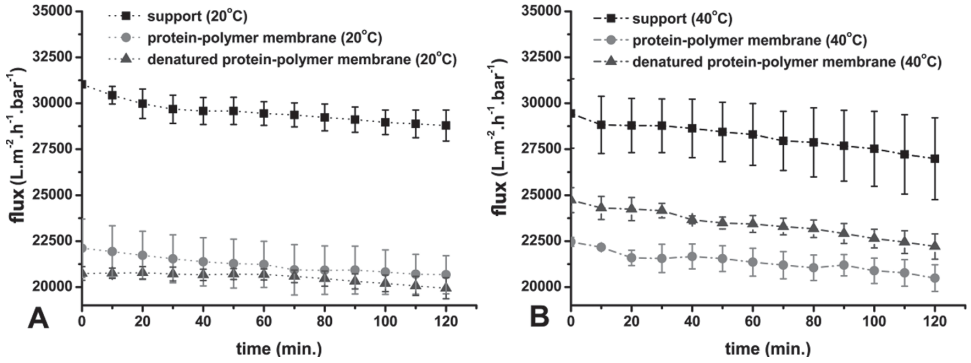

Figure 4. Water flux over time using the PEG-mixture was determined for the support, the support with protein-polymer membrane and the support with protein-polymer membrane after denaturation at a TMP of 9 mbar. Measurements were performed at 20 °C (below LCST) and 40 °C (above LCST). Plots represent an average of three separate flux over time measurement and errors are derived as the deviation from the average.

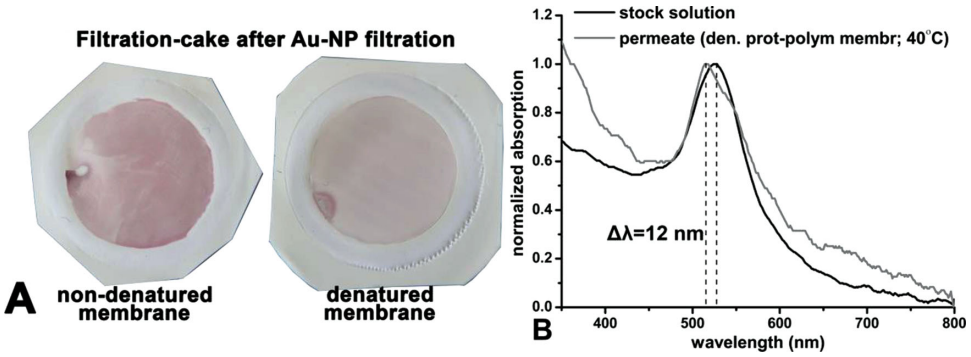

Figure 5. A) photograph of the membrane used in gold nanoparticle filtration experiments at 40 °C without denaturation (left) and with denaturation (right) of the ferritin. B) Absorption spectra of the gold nanoparticle stock solution before and after filtration experiments. The low concentration of particles in the permeate gives rise to a lower signal-to-noise ratio.

very thin and polymer agglomeration can occur which would open the matrix for water to pass while larger structures are repelled. This would explain why still high flux is observed at elevated temperatures. As a result, above the LCST the flux for the denatured membrane increases compared to the non-denatured membrane. This indicates that after the collapse of the polymer matrix the water transport can only take place through the pores created via denaturation of the ferritin. In addition, since the denatured protein can no longer act as a cross-linking point between the matrix, the peptide fragments which are left after denaturation are being pulled apart during the collapse of the polymer matrix creating a more open structure leading to a facilitated transport. The flux found here is much higher and is associated to pressures significantly lower than for other membrane systems which are considered ultra-thin (in the range of 20–50 nm).[37–39] Upon analysis of the collected permeate, no selectivity was found towards the different molecular weight PEG. Most likely, the polymers are too small and too flexible and therefore able to penetrate the protein-polymer membrane both before and after denaturation of the ferritin. However, the flux analysis provides important insights into the membrane behavior and stability at different temperatures.

2.2.3. Membrane Selectivity Towards Nanoparticles

For further testing of the protein-polymer membrane, gold nanoparticles were chosen as a more rigid analyte. In earlier studies this proved a suitable method to determine selectivity using TEM and spectrophotometry.[11,40] For this a single stock solution of a mixture of gold nanoparticles in the range of 2–30 nm was used in all experiments. The filtration was performed in the same setup as was described before at 40 °C since above the LCST the most significant difference in permeation was observed. The feed was analyzed by TEM and spectrophotometry and compared with the permeate collected through the denatured and non-denatured protein-polymer membrane. A difference was immediately detected between the denatured and the non-denatured membrane with respect to the color of the permeate and the color of the membrane surface. In the case of the non-denatured protein-polymer membrane, the permeate was colorless and no absorption using spectrophotometry could be detected even after extensively concentrating the volume. Furthermore, the surface of the membrane was more discolored (**Figure 5**A) as compared to the surface of the denatured protein-polymer membrane. For the denatured membrane, the absorption spectrum of the permeate displayed a shift of 12 nm towards lower wavelengths for the maximum absorption intensity in comparison to the absorption of the stock solution. As larger particles display the plasmon absorption band at higher wavelengths, this shift indicates that larger particles do not pass through the membrane as readily as the smaller particles (Figure 5B). This was confirmed by TEM analysis where the amount of particles of a specific size were compared before and after filtration. As listed in **Table 1**, the composition changes and the relative amount of particles in the range between 20–30 nm was reduced by 56%, 7–12 nm reduced by 8% and 2–5 nm increased by 8%. Even though, there is no absolute cut-off in size, there is a selectivity towards smaller particles to permeate which results in an accumulation of smaller particles and a depletion of larger particles. Qualitative investigations on the membrane after filtration displayed indeed that predominantly the larger particle remain on the membrane surface (Figure S8, Supporting Information).

3. Conclusion

We have demonstrated a new concept for the preparation of ultra-thin, large area, highly flexible membranes in which a

Table 1. Change in gold nanoparticle composition upon filtration across the denatured protein-polymer membrane at 40 °C. Used TEM images shown in S7. Average size and Standard Deviation (S.D.) based on absolute particle counts. Substantial lowering of S.D. indicates significant reduction of number of particles with larger diameter.

	Stock solution	Permeate denatured prot.-polym. membrane (40 °C)	Relative difference
Au-NP size [nm]	Size fraction [%]	Size fraction [%]	Size fraction [%]
2–5	78	84	+8
7–12	13	12	–8
20–30	9	4	–56
Average/ Standard Dev.	5.3 nm/4.4 nm	4.3 nm/3.0 nm	32% lowering S.D.

protein structure is used as a sacrificial template which providing a porous membrane after denaturation. The conditions for removal of protein templates are milder than conventional inorganic templates which use highly corrosive solutions. Additionally the size control of the sacrificial template is predetermined and impeccably reproducible compared to synthetic (in)organic particle templates. In this case ferritin was used as a model protein, however, this approach holds the potential that in principle any protein with varying size and shape could be employed. The membrane produced after denaturation of the ferritin displays different permeation properties below and above the LCST of the used polymer matrix. Such type of permeation control via external stimuli has previously also been observed using polymeric and polymeric-nanoparticle based membranes.[48,49] In this particular case an opening of the pore was induced but it can also be imagined that this may also facilitate membrane cleaning simply by lowering the temperature and therefore completely opening the structure and removing any selectivity. Denaturation is performed under relatively "harsh" chemical conditions and in order to make it more applicable, membranes are developed which will omit the denaturing step, for example, by using a channel protein, which has previously been used in polymersome systems and lipid membranes.[41–43] In addition, this approach also provides the possibility to incorporate various innovations like pore-stoppers and catalysts which introduces additional functionality to the membrane. The low pressure needed for these membrane would allow applications in e.g. pathogen removal from aqueous environments especially in combination with peptide strands and or proteins residing inside the membrane matrix. Particularly, in a cross-flow membrane setup which operate at low pressures. Although, future approaches would also include the preparation of more impermeable polymer matrices towards water which would allow higher pressures to be used.

4. Experimental Section

Horse Spleen ferritin was purchased from Fluka. *2*-Bromoisobutyric acid (BIBA) (99%, Aldrich), *N*-hydroxysuccinimide (NHS) (Aldrich, 98%), *1,3*-dicyclohexal carbodiimide (DCC) (Aldrich, 99%) and DMF (peptide grade, Biotech) were used as purchased. NIPAAm (99%, Aldrich) was purified by two successive recrystallizations in a mixture of *n*-hexane and benzene (4:1 v:v). CuBr (98%, Aldrich) was purified by stirring in acetic acid overnight. After filtration, it was washed with ethanol and ether and then dried in vacuum, $CuBr_2$ (99%, Aldrich) was used as purchased. Me_6TREN was prepared as described by Ciampolini.[44] The photo-cross-linker monomer *2*-(dimethyl maleinimido)-*N*-ethyl-acrylamide (DMIAAm) was synthesized according to the procedure reported by Kuckling et al.[45] Gold nanoparticles used in the size-exclusion experiments were synthesized according to literature procedure using cetyltrimethylammonium bromide as the stabilizing agent.[46] For scanning force microscopy (SFM) a Veeco Instruments SFM was used operating on Nanoscope software. Measurement were performed in tapping mode in air using a SiN-tip at slow scan-rates (1.05 Hz) at room temperature. Circular dichroism experiments were performed on a dichrograph On-Line Instrument System Inc. CD measurements were performed on ferritin and ferritin-polymer conjugates in solution at room temperature. An OLIS 17 ellipsometer optical analytic MM-SPEL-VIS was used for layer thickness determination. For analysis the Visu EL program was used using standardized settings of organic layer (Refractive index: 1.45) on SiO_2 (n, k) on Si. Gel electrophoresis was performed using a BIORAD PROTEAN system. Inter-particle cross-linking was performed with a 400 W UV-Lamp Panacol 400 F. TEM-visualization was performed using a Zeiss Libra plus transmission electron microscope. Samples for TEM were prepared by placing a drop of solution onto a carbon-coated Cu-grid and blotting away excess liquid after a minute. TEM imaging did not display any aggregate formation and it can be assumed that therefor this also does not occur in solution. UV-Vis measurements were performed on an EVOLUTION 300 UV–Visible spectrometer. For fluorescence microscopy imaging a Keyence instrument BZ-8100E was used.

Conjugate Synthesis: The synthesis of the ferritin macro-initiator was performed as reported by Zeng et al.[47] The quantity of *N*-hydroxysuccinimidyl *2*-bromo-isobutyrate (NHS-BIBA) needed for the reaction amounts 7200 molar equivalent with respect to ferritin. The 100-fold excess of NHS-BIBA with respect to the 72 amino groups per ferritin was chosen to obtain good conversion. NHS-BIBA was mixed with the corresponding amount of a ferritin stock-solution with an estimated concentration of 50 mg mL^{-1}. The concentration of ferritin was determined from the UV absorption in high purity water at λ = 280 nm (ε_{280} = 4.8 × 10^5 M^{-1} cm^{-1}). First, NHS-BIBA was dissolved in a 5:1 mixture of phosphate buffer (PBS, pH 8.5) and dimethylformamide (DMF). The ferritin stock-solution was added subsequently. The reaction mixture was shaken over night at 4 °C. After the reaction the mixture was dialyzed (cut-off value 3 kDa) in PBS at pH 8.5 to remove excess initiator. In the subsequent reaction step the ATRP of NIPAAm and DMIAAm was conducted with a molar ratio of NIPAAm/DMIAAm/Ferritin-BIBA (macro-initiator)/Cu(I)/Cu(II)/ligand = 5.3/0.27/0.0012/0.32/0.16/0.6. The amount of the individual reagents used for each reaction 20 mL of a 1 mg/mL ferritin-BIBA solution, NIPAAm 600 mg, DMIAAm 60 mg, Cu(I)Br 46 mg, Cu(II) Br_2 36 mg, Me_6TREN 160 µL. Cu(I)Br, Cu(II)Br2 and Me6TREN were dissolved in high purity water. NIPAAm and DMIAAm were mixed into the ferritin-BIBA macro-initiator solution. Both solutions were degassed under nitrogen flow for 60 min under cooling at 0 °C. Afterwards, the corresponding volume of the copper-ligand solution was added to the monomer/macro-initiator solution. The reaction mixture was allowed to react for 24 h at 4 °C under continuous shaking. To remove the catalyst the solution was dialyzed (cut-off value 3 kDa) against PBS with pH 7.4. In the case of the fluorescently labeled polymer, the same procedure was followed in combination with fluorescein-acrylate 1% w/w with respect to NIPAAm. For the membrane experiments, the conjugate solution was further dialyzed against MilliQ water to circumvent salt crystal formation during drying.

Drying-mediated Self-Assembly: For drying-mediated self-assembly, a drop of the ferritin-polymer conjugate solution, diluted with high purity water, was placed onto a support. Silica wafers, TEM grids and porous polycarbonate supports (pore-size 100 nm) and polyethersulfone supports (pore-size 200 nm) were used. The silica wafers were cut into 1 cm × 1 cm large pieces and stored in toluene to remove organic impurities. Before use, the wafers were cleaned with a snow-jet. Porous supports (hydrophilized polyethersulfone) were placed onto a teflon sheet which was used to prevent the conjugate solution from running into the pores. 2 mL of MilliQ-water was placed inside the "O"-ring (Ø = 25 mm) which was placed on top of the porous support with a thin layer of grease between the contact to prevent solution escaping from the center of the "O"-ring. Subsequently, 20 µL of a 1 mg/mL solution of ferritin-polymer conjugate was spread on top of the MilliQ-water. The system was irradiated with UV-light while cooling at 0 °C until the water was completely evaporated (approx. 3 h). For the permeation experiments, a polyethersulfone membrane (pore size 200 nm) was used.

Denaturation of Ferritin: Denaturing ferritin inside the membranes was achieved with aqueous solutions of guanidinium chloride (7 M, pH 4.4) or urea (8 M). The substrate holding the self-assembled protein-polymer membrane was covered with 2 mL of a solution containing the denaturing agent. The samples were heated in an oven at 90 °C for 3 h. Afterwards, the surface was gently yet thoroughly washed with

MilliQ-water. Denaturation experiments to obtain optimal conditions as was determined by CD were performed in solution and extrapolated to suitable for surface confined denaturation.

Permeation Experiments: To test the performance and flow rates of the membranes, permeation experiments were carried out using an in house-designed flow station specifically designed for the experiments. The membrane holder had three inlets on each side of the membrane-housing: one for feed/permeate at the top/bottom to maintain a straight flow pattern, one for pressure sensors, and one for adding analytes into the housing. The membrane was fixed between two metal meshes with two "O"-rings for sealing. A magnetic bar was placed in the top chamber (feed side) and stirred at 500 rpm to prevent concentration polarization. Four screws were used to connect the two chambers and provide a sufficient contact pressure for the "O"-rings to seal the system. Because the filtration active membrane was a very thin layer, only hydrostatic pressure was applied in the permeation experiments. A cylindrical container made of polytetrafluoroethylene with a diameter of 120 mm and an attached tube contained the feed solution. The hydrostatic pressure was adjusted via the height of the feed solution in the container until the desired trans-membrane pressure (TMP) was achieved; for the higher pressures, lifting platforms were available to elevate the container, creating trans-membrane pressures up to 51 mbar. Attached to the permeate side of the housing was a container on a balance measuring the mass of permeate. A computer running a self-written data acquisition software (DASYlab, National Instruments, Austin, TX, USA) was used to collect data such as permeate mass, pressure on feed and permeate side and room temperature. Different types of permeation experiments were carried out to examine different characteristics of the membrane. Pure water was used as feed solution for permeation experiments to determine the flux of the membrane at different pressures. Support membranes without coating and protein-polymer coated membranes were measured for 15 minutes at each given trans-membrane pressure. For the determination of the size selectivity of the membrane, permeation experiments with PEG solution and gold nanoparticles (AuNP) were carried out at a constant TMP of 9 mbar, afterwards a permeate sample was taken for analysis. Due to the phase transition of polyNIPAAm above temperatures of 32–35 °C experiments for filtration were carried out at feed solution temperatures of 20 °C and 40 °C. For the permeation experiments with gold nanoparticles, a TMP of 9 mbar and a feed temperature of 40 °C was used. The permeation rates were then compared to those of the previous permeation tests with ultrapure water to ensure the correct operation of the membrane. The gold nanoparticles, which existed in size classes of 2–5 nm, 7–12 nm and 20–30 nm were mixed and used as the feed solution. To create a feed solution with approximately the same number of small, medium and large particles, the volume of the solution containing the large particles was larger than that of the small particles (3 parts small, 4 parts medium, and 5 parts large particles). 1 mL of this mixture was then injected directly into the feed side of the membrane housing. Then the experiment was carried on for 20 mL of flow volume, the permeate was collected for analysis by absorption spectroscopy and TEM.

Supporting Information

Supporting Information is available from the Wiley Online Library or from the author.

Acknowledgements

P.v.R., M.T., and C.K. contributed equally to this work. The authors acknowledge Dr. Edward Rochford for proof-reading the manuscript and Prof. Dr. Matthias Wessling for graciously providing the lab space and equipment for flux determination. The Alexander von Humboldt foundation (P.v.R.) and the VolkswagenStiftung in the framework of the Lichtenberg Program (A.B.) are kindly acknowledged for financial support.

Received: June 20, 2014
Revised: July 7, 2014
Published online: September 1, 2014

[1] Y. Wang, F. Li, *Adv. Mater.* **2011**, *23*, 2134.
[2] E. Jackson, M. Hillmyer, *ACS Nano* **2010**, *4*, 3548.
[3] P. van Rijn, M. Tutus, C. Kathrein, L. Zhu, M. Wessling, U. Schwaneberg, A. Böker, *Chem. Soc. Rev.* **2013**, *42*, 6578.
[4] M. Schnietz, A. Turchanin, C. T. Nottbohm, A. Beyer, H. H. Solak, P. Hinze, T. Weimann, A. Gölzhäuser, *Small* **2009**, *5*, 2651.
[5] J. He, X.-M. Lin, H. Chan, L. Vuković, P. Král, H. M. Jaeger, *Nano Lett.* **2011**, *11*, 2430.
[6] J. He, P. Kanjanaboos, N. L. Frazer, A. Weis, X.-M. Lin, H. M. Jaeger, *Small* **2010**, *6*, 1449.
[7] Y. Lin, H. Skaff, A. Böker, A. D. Dinsmore, T. Emrick, T. P. Russell, *J. Am. Chem. Soc.* **2003**, *125*, 12690.
[8] X. Peng, J. Jin, Y. Nakamura, T. Ohno, I. Ichinose, *Nat. Nanotechnol.* **2009**, *4*, 353.
[9] J. T. Russell, Y. Lin, A. Böker, L. Su, P. Carl, H. Zettl, J. He, K. Sill, R. Tangirala, T. Emrick, K. Littrell, P. Thiyagarajan, D. Cookson, A. Fery, Q. Wang, T. P. Russell, *Angew. Chem. Int. Ed.* **2005**, *44*, 2420.
[10] D. Carvajal, R. Bitton, J. R. Mantei, Y. S. Velichko, S. I. Stupp, K. R. Shull, *Soft Matter* **2010**, *6*, 1816.
[11] E. Krieg, H. Weissman, E. Shirman, E. Shimoni, B. Rybtchinski, *Nat. Nanotechnol.* **2011**, *6*, 141.
[12] P. Zavala-Rivera, K. Channon, V. Nguyen, E. Sivaniah, D. Kabra, R. H. Friend, S. K. Nataraj, S. A. Al-Muhtaseb, A. Hexemer, M. E. Calvo, H. Miguez, *Nat. Mater.* **2012**, *11*, 53.
[13] W. A. Phillip, B. O'Neill, M. Rodwogin, M. A. Hillmyer, E. L. Cussler, *ACS Appl. Mater. Interfaces* **2010**, *2*, 847.
[14] M. Nallani, S. Benito, O. Onaca, A. Graff, M. Lindemann, M. Winterhalter, W. Meier, U. Schwaneberg, *J. Biotechnol.* **2006**, *123*, 50.
[15] P. Tanner, O. Onaca, V. Balasubramanian, W. Meier, C. G. Palivan, *Chem. Eur. J.* **2011**, *17*, 4552.
[16] M. Kumar, M. Grzelakowski, J. Zilles, M. Clark, W. Meier, *Proc. Natl. Acad. Sci.* **2007**, *104*, 20719.
[17] O. Onaca, R. Enea, D. W. Hughes, W. Meier, *Macromol. Biosci.* **2009**, *9*, 129.
[18] F. Meng, Z. Zhong, J. Feijen, *Biomacromolecules* **2009**, *10*, 197.
[19] C. G. Palivan, O. Fischer-Onaca, M. Delcea, F. Itel, W. Meier, *Chem. Soc. Rev.* **2012**, *41*, 2800.
[20] A. Dzgoev, K. Haupt, *Chirality* **1999**, *11*, 465.
[21] S. B. Lee, D. T. Mitchell, L. Trofin, T. K. Nevanen, H. Söderlund, C. R. Martin, *Science* **2002**, *296*, 2198.
[22] I. Vlassiouk, P. Y. Apel, S. N. Dmitriev, K. Healy, Z. S. Siwy, *Proc. Natl. Acad. Sci.* **2009**, *106*, 21039.
[23] H. D. Tong, H. V. Jansen, V. J. Gadgil, C. G. Bostan, E. Berenschot, C. J. M. Van Rijn, M. Elwenspoek, *Nano Lett.* **2004**, *4*, 283.
[24] N. C. Mougin, P. van Rijn, H. Park, A. H. E. Müller, A. Böker, *Adv. Funct. Mater.* **2011**, *21*, 2470.
[25] C. W. Pester, A. Konradi, B. Varnholt, P. van Rijn, A. Böker, *Adv. Funct. Mater.* **2012**, *22*, 1724.
[26] K. Ozlem Nazli, C. W. Pester, A. Konradi, A. Böker, P. van Rijn, *Chem. Eur. J.* **2013**, *19*, 5586.
[27] S. C. Andrews, P. Arosio, W. Bottke, J. F. Briat, M. von Darl, P. M. Harrison, J. P. Laulhère, S. Levi, S. Lobreaux, S. J. Yewdall, *J. Inorg. Biochem.1992, 47*, 161.

[28] Y. Hu, D. Samanta, S. S. Parelkar, S. W. Hong, Q. Wang, T. P. Russell, T. Emrick, *Adv. Funct. Mater.* **2010**, *20*, 3603.
[29] B. Fernández, N. Gálvez, P. Sánchez, R. Cuesta, R. Bermejo, J. M. Domínguez-Vera, *J. Biol. Inorg. Chem.* **2008**, *13*, 349.
[30] P. van Rijn, H. Park, K. Özlem Nazli, N. C. Mougin, A. Böker, *Langmuir* **2013**, *29*, 276.
[31] X. Huang, M. Li, D. C. Green, D. S. Williams, A. J. Patil, S. Mann, *Nat. Commun.* **2013**, *4*, 2239.
[32] P. van Rijn, N. C. Mougin, A. Böker, *Polymer* **2012**, *53*, 6045.
[33] P. D. Hempstead, S. J. Yewdall, A. R. Fernie, D. M. Lawson, P. J. Artymiuk, D. W. Rice, G. C. Ford, P. M. Harrison, *J. Mol. Biol.* **1997**, *268*, 424.
[34] P. van Rijn, N. C. Mougin, D. Franke, H. Park, A. Böker, *Chem. Commun.* **2011**, *47*, 8376.
[35] J. K. Holt, H. G. Park, Y. Wang, M. Stadermann, A. B. Artyukhin, C. P. Grigoropoulos, A. Noy, O. Bakajin, *Science* **2006**, *312*, 1034.
[36] C. C. Striemer, T. R. Gaborski, J. L. McGrath, P. M. Fauchet, *Nature* **2007**, *445*, 749.
[37] Y. Han, Z. Xu, C. Gao, *Adv. Funct. Mater.* **2013**, *23*, 3693.
[38] B. Li, W. Liu, Z. Jiang, X. Dong, B. Wang, Y. Zhong, *Langmuir* **2009**, *25*, 7368.
[39] L. Y. Jiang, Y. Wang, T.-S. Chung, X. Y. Qiao, J.-Y. Lai, *Prog. Polym. Sci.* **2009**, *34*, 1135.
[40] D. Z. Fang, C. C. Striemer, T. R. Gaborski, J. L. McGrath, P. M. Fauchet, *Nano Lett.* **2010**, *10*, 3904.
[41] O. Onaca, M. Nallani, S. Ihle, A. Schenk, U. Schwaneberg, *Biotechnol. J.* **2006**, *1*, 795.
[42] P. Broz, S. Driamov, J. Ziegler, N. Ben-Haim, S. Marsch, W. Meier, P. Hunziker, *Nano Lett.* **2006**, *6*, 2349.
[43] M. Tutus, S. Kaufmann, I. M. Weiss, M. Tanaka, *Adv. Funct. Mater.* **2012**, *22*, 4873.
[44] M. Ciampolini, N. Nardi, *Inorg. Chem.* **1966**, *5*, 41.
[45] L. Ling, W. D. Habicher, D. Kuckling, H.-J. Adler, *Des. Monomers Polym.* **1999**, *2*, 351.
[46] R. Contreras-Cáceres, J. Pacifico, I. Pastoriza-Santos, J. Pérez-Juste, A. Fernández-Barbero, L. M. Liz-Marzán, *Adv. Funct. Mater.* **2009**, *19*, 3070.
[47] Q. Zeng, T. Li, B. Cash, S. Li, F. Xie, Q. Wang, *Chem. Commun.* **2007**, *14*, 1453.
[48] L. Ouyang, R. Malaisamy, M. L. Bruening, *J. Membrane Sci.* **2008**, *310*, 76.
[49] A. G. Skirtach, P. Karageorgiev, M. F. Bédard, G. B. Sukhorukov, H. Möwald, *J. Am. Chem. Soc.* **2008**, *130*, 11572.